https://doi.org/10.5194/essd-2026-11
Preprint. Discussion started: 16 March 2026

Open Access Earth System Science Data Discussions

A field dataset from replicated prescribed fire experiments on wildland fire behaviour and fire–atmosphere interactions

Nicholas S. Skowronski[1], Xindi Bian[2], Zakary J. Campbell-Lochrie[3], Joseph J. Charney[2], Kenneth L. Clark[4], Jason A. Cole[4], Julia Defeo[5], Giovanni Di Cristina[6], Alexis I. Everland[7], Michael R. Gallagher[4], Rory M. Hadden[3], Warren E. Heilman[2], John L. Hom[4], Seong-kyun Im[8], Michael T. Kiefer[9], Robert L. Kremens[10], William E. Mell[11], Eric V. Mueller[6], Matthew M. Patterson[4], Ali Rangwala[10], Joseph Seitz[9], Albert J. Simeoni[10], Carlos Walker-Ravena[3], and Shiyuan Zhong[9]

[1]National Office, Fire and Aviation Management, Washington, DC, USA
[2]U.S. Forest Service, Northern Research Station, Lansing, MI, USA
[3]University of Edinburgh, Edinburgh, UK
[4]U.S. Forest Service, Northern Research Station, New Lisbon, NJ, USA
[5]Ohio State University, Columbus, OH, USA
[6]National Institute of Standards and Technology, Gaithersburg, MD, USA
[7]New Jersey Forest Fire Service, Trenton, NJ, USA
[8]Korean University, Seoul, South Korea
[9]Michigan State University, East Lansing, MI, USA
[10]Worcester Polytechnic Institute, Worcester, MA, USA
[11]U.S. Forest Service, Pacific Northwest Research Station, Seattle, WA, USA

Correspondence to: Shiyuan Zhong (zhongs@msu.edu)

Abstract. We present a spatially and temporally resolved dataset characterizing combustion dynamics, fire behaviour, and associated environmental variables from thirty-five replicated prescribed fire experiments conducted between March 2018 and May 2019 on 10 m × 10 m burn plots at the U.S. Forest Service Silas Little Experimental Forest in the New Jersey Pinelands, USA. The experiments were designed to quantify the physical processes driving combustion, flame propagation, and energy exchange, bridging the gap between small-scale laboratory studies and large-scale prescribed fires. The dataset provides synchronized, multi-instrument observations of high frequency three-dimensional wind, temperature, pressure, fire radiative power, gas concentrations, fuel moisture, and mass loss, along with pre- and post-burn terrestrial LiDAR scans of fuel structure. These data capture key interactions among fuels, atmosphere, and combustion processes at a scale relevant to wildland fire behaviour. The dataset supports development and validation of coupled fire–atmosphere and combustion models, as well as analyses of radiative energy transfer and fuel consumption dynamics. All data are publicly available through the U.S. Forest Service Research Data Archive as an open-access benchmark resource for advancing process-level understanding and model evaluation in wildland fire science.

https://doi.org/10.5194/essd-2026-11
Preprint. Discussion started: 16 March 2026

Open Access Earth System Science Data Discussions

1 Introduction

Understanding the physical processes that govern fire behaviour during prescribed burns across diverse ecosystems, particularly in pine- and pine–oak–dominated environments, remains a central challenge in fire science (Hiers et al., 2020; Cruz et al., 2025). Current knowledge of combustion dynamics, heat transfer, and fire–atmosphere interactions is derived primarily from studies conducted at two distinct scales: small-scale laboratory experiments and large-scale operational prescribed burns.

At the smallest scale, controlled laboratory burns enable precise manipulation of fuel and environmental conditions and have yielded valuable insights into ignition, heat transfer, and flame propagation (El Houssami et al., 2016; Li et al., 2020; Butler, et al., 2020; Finney et al., 2021; Mueller et al., 2022; Li et al., 2024; Saha and Cobian-Iñiguez, 2025). However, these experiments cannot replicate the spatial variability of fuel loading, structure, and moisture, nor the dynamic meteorological conditions that strongly influence fire behaviour in the field. At the opposite end of the spectrum, large-scale prescribed burns capture the full complexity of fire–atmosphere coupling under realistic conditions (Hinzman, et al., 2003; Ottmar et al. 2006; Prichard et al., 2019). Field campaigns employing tower- and surface-based measurements have revealed emergent behaviours such as fire-induced up- and down-drafts, horizontal inflow behind flame fronts, and turbulence enhancement within buoyant plumes (Heilman et al., 2017, 2019, 2021a; Clements et al., 2019; Clark et al., 2020; Katurji et al., 2022). These management-scale field campaigns further elucidated the diverse impacts of prescribed fires on ecosystems, encompassing changes in vegetation, carbon storage, emissions, and soil processes such as runoff and erosion (Linddas, et al., 2020; Francos and Ubeda, 2021; Valco and Deak, 2021; Agbeshie, et al., 2022; Carrà et al., 2022; Butler et al., 2025). Yet, despite their value, the multitude of interacting processes during operational burns makes it difficult to isolate controlling mechanisms or to obtain spatially resolved measurements, while fuel and thermal data are often coarse in scale (Hiers et al., 2020; Heilman, 2021b).

Bridging the gap between these two experimental scales is therefore essential for advancing both empirical and physics-based fire behaviour models. Important questions remain: which turbulence and circulation features occur consistently across scales, and which are emergent behaviours linked to fire intensity or fuel configuration? For instance, the inflow of cool air into the backs of flame fronts has been observed in more intense head or flanking fires but the signal is weak at best in low-intensity backing fires (Mueller et al., 2018; Heilman et al., 2021a; Seitz, et al. 2024). Understanding when and under what conditions such circulations develop is critical for predicting fire spread, plume evolution, and heat transfer processes.

Physics-based models such as FIRETEC (Linn et al., 2002), WFDS (Mell et al., 2007), and QUIC-FIRE (Linn et al., 2020) have the potential to represent these coupled processes, but their accuracy depends on the availability of high-quality, spatially explicit observational datasets for initialization, parameterization, and validation (Liu et al., 2019). The scarcity of replicated, intermediate-scale field experiments with dense instrumentation remains a major limitation.

To address this gap, we conducted a series of highly instrumented, replicated intermediate-scale (10 m × 10 m) prescribed burns at the U.S. Forest Service Silas Little Experimental Forest in New Jersey, USA, between March 2018 and May 2019. Supported by the U.S. Department of Defence Strategic Environmental Research and Development Program (SERDP, Project

https://doi.org/10.5194/essd-2026-11
Preprint. Discussion started: 16 March 2026

RC-2641), these experiments bridge the laboratory–field divide by combining the control and replication of small-scale burns with the realism of operational prescribed fires. The experimental design contrasts dormant- versus growing-season conditions and natural versus augmented fuel loads, thereby capturing variability in fuel structure, combustion environment, and meteorological forcing.

This dataset provides a unique opportunity to examine fine-scale fire–atmosphere interactions in low-intensity prescribed fires under controlled yet field-realistic conditions. By integrating detailed measurements of meteorology, thermal structure, and fuel characteristics, it supports new analyses of turbulence dynamics, convective heat fluxes, and the coupling between fire spread and atmospheric processes. Beyond advancing physical understanding, the dataset offers a foundation for testing and improving physics-based fire behaviour models and for facilitating cross-scale comparisons with both laboratory and landscape-scale studies.

2 Methods

2.1 Experimental site

The Silas Little Experimental Forest is a U.S. Forest Service Northern Research Station research facility located in New Lisbon, New Jersey, USA (39.9177° N, 74.5964° W), within the New Jersey Pinelands National Reserve—a 380 000 ha region of pine–oak forest characteristic of the Atlantic Coastal Plain (Fig.1). The site is characterized by flat terrain, well-drained sandy soils, and vegetation dominated by pitch pine (*Pinus rigida*) and oak species including *Quercus montana*, *Q. velutina*, *Q. alba*, and *Q. marilandica*.

Experimental burns were conducted within a 5 acre plantation of *P. rigida* and *P. taeda* established in 1965 (Fig. 1). The stand's uniform structure, flat topography, and history of prescribed fire provide controlled and repeatable conditions for fire–atmosphere process studies.

2.2 Experimental design

A total of 35 prescribed burns were conducted on 10 m × 10 m plots between March 2018 and May 2019 to quantify combustion dynamics, energy release, and coupled flow processes under field-realistic conditions. Each plot was instrumented with four overhead aluminum trusses and a central tower, supporting dense arrays of sensors measuring wind, temperature, pressure, radiation, and gas concentration. Burn conditions were designed to represent contrasting seasonal (dormant vs. growing) and fuel scenarios (natural vs. augmented pine–oak mixtures). The first 10 burns were performed on separate plots with naturally accumulated litter, whereas Burns 11–35 were conducted on a reusable plot where dried fuels of known mass were evenly distributed before each experiment. For Burns 1–10, fuel loading was determined via destructive sampling around the plot perimeter. For Burns 11–35, pre-weighed fuels were applied to achieve target loadings of 0.48–1.44 kg m^{-2}, with gravimetric fuel moisture contents ranging from 4% to 12%.

https://doi.org/10.5194/essd-2026-11
Preprint. Discussion started: 16 March 2026

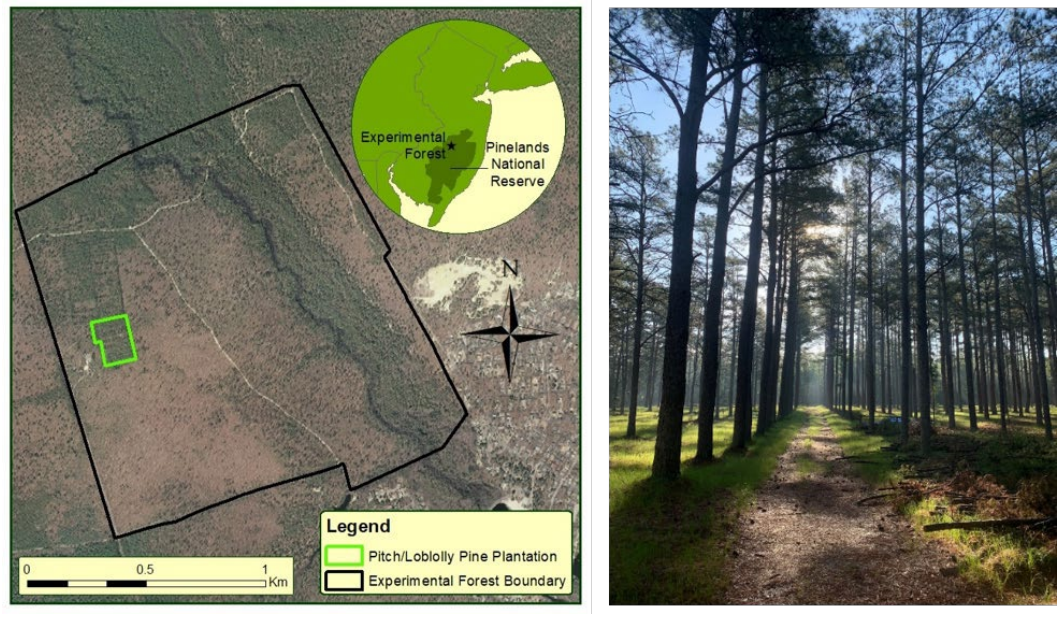

Figure 1: Experiment site in pitch/loblolly pine plantation at the Silas Little Experimental Forest, New Lisbon, NJ, USA

Across all burns, fires were initiated using a length of clothesline soaked in an accelerant. Two personnel held the line aloft from opposite corners of the plot; the line was ignited and then lowered to the ground, allowing the entire edge of the plot to ignite simultaneously (Fig. 2). Each burn lasted approximately 10–20 minutes and encompassed the full sequence of ignition, active flaming, and smoldering.

Figure 2: Typical linear ignition using 10 m cord soaked in accelerant

https://doi.org/10.5194/essd-2026-11
Preprint. Discussion started: 16 March 2026

Open Access Earth System Science Data Discussions

2.3 Plot infrastructure and major instrumentation

Four overhead aluminum trusses were mounted on steel tripods above the burn unit to minimize disturbance while supporting instrumentation above the 10 m × 10 m burn plot (Fig. 3). A 10-m central tower provided mounting for infrared cameras and reference sensors (Fig. 3). Instrumentation targeted key physical domains of the combustion environment:

- Flow and turbulence: three-dimensional (3D) wind velocity and virtual temperature from sonic anemometers at 2.5 m (burns 1-22) or 3.0 m (burns 23-35) height level.
- Temperature and pressure: Vertical thermocouple arrays and pressure sensors co-located with anemometers.
- Radiation and heat flux: Dual-band infrared radiometers measuring fire radiative power and convective energy flux.
- Combustion gases: Transportable Analyzer for Calorimetry Outside (TACO) system measuring CO_2, CO, and O_2 concentrations and exhaust flow.
- Fuel consumption: Load cells quantifying mass loss during combustion.
- Optical and structural data: Infrared (IR) video cameras and terrestrial laser scans (TLS) capturing flame structure, fuelbed structure, and fine-scale topography.

All instruments were synchronized via GPS time and recorded with Campbell Scientific data loggers (CR3000, CR6, or CR1000). A summary of the instrumentation and their specifications is provided in Table 1.

3 Data acquisition

Building on the experimental design described above, the dataset includes high-frequency in-situ measurements of wind, temperature, pressure, radiation, and gas concentrations, as well as remote sensing observations of flame spread and fuel structure. All measurement subsystems were time-synchronized and spatially referenced, enabling integration across scales for model evaluation and process-based analysis. The following subsections describe the data collection methods by measurement type.

3.1 Air flow, temperature, and pressure measurements

Mean air flow and turbulence were characterized using 3D sonic anemometers (Model 81000V, R.M. Young Inc., Traverse City, MI, USA) deployed in a 4 × 4 grid spanning the 10 m × 10 m burn plots (Figs. 3, 4). Sensors were typically positioned 2.5–3.0 m above the fuelbed and at 10 m on the central tower. In two burns (Burns 7 and 8), an alternative configuration included two vertical levels (1.5 m and 3.5 m) on Trusses B and C to resolve vertical turbulence structure. These sonic anemometers recorded zonal (east-west), meridional (north-south), and vertical wind speeds and virtual temperature.

https://doi.org/10.5194/essd-2026-11
Preprint. Discussion started: 16 March 2026

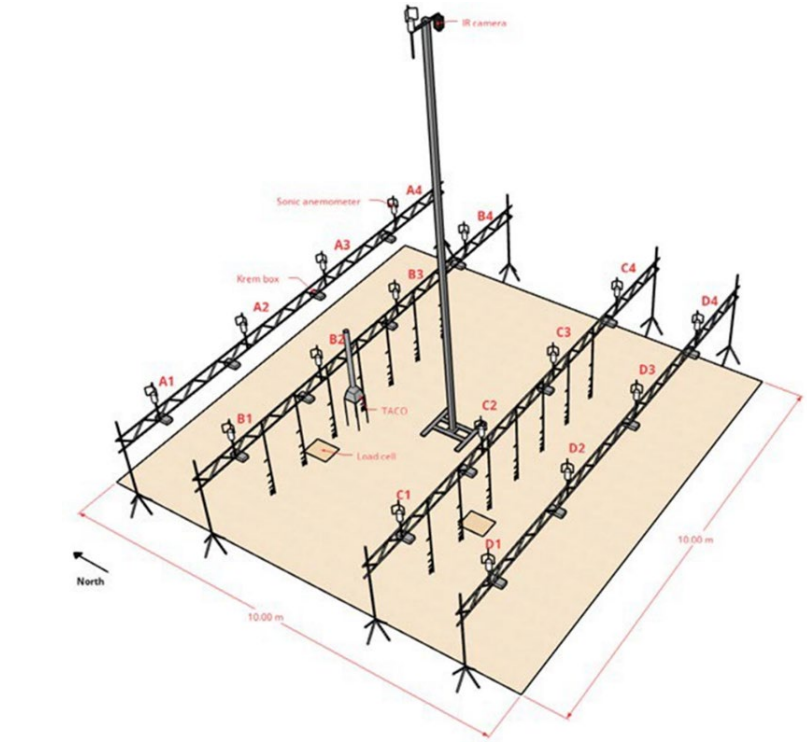

Figure 3: Illustration of the burn plot layout. Sensor locations were denoted by truss designator (e.g., A-D) and a position number, beginning with "1" in the western side of the plot and ending with "4" at the eastern side of the plot.

High-frequency fire temperature measurements were made using Type K thermocouples (KMTXL-IOM25G-150, Omega Engineering Inc., Norwalk, CT, USA) arranged in vertical arrays with sensors at 0, 5, 10, 20, 30, 50, and 100 cm above the fuelbed (Figs. 3, 4, 5). The thermocouple arrays were mounted on Trusses B and C. Experiments 1–6 included four arrays (two per truss); from Experiment 7 onward, additional arrays were added to achieve 1.5 m horizontal spacing, yielding 14 arrays in total.

Eight air pressure sensors (Bosch BMP180/BMP280, Bosch Sensortec, Reutlingen, Germany) recorded high-frequency variations in atmospheric pressure for Burns 1–19. Sensors were collocated with the anemometers at heights of 2.5–3.0 m (or 1.5 m and 3.5 m in Burns 7–8) (Figs. 3, 4).

All measurements above were logged at 10 Hz using either CR3000 or CR6 data loggers (Campbell Scientific, Inc., Logan, UT, USA). Together, these measurements provide detailed characterization of the mean and fluctuating components of flow, temperature, and pressure during the burns.

https://doi.org/10.5194/essd-2026-11
Preprint. Discussion started: 16 March 2026

3.2 Fire spread and radiative power

Fire spread and radiative energy output were quantified using a suite of infrared and optical instruments. Overhead measurements were collected with a FLIR A655SC infrared camera (FOL6 100.0–650.0 °C lens; FLIR Systems Inc., Wilsonville, OR, USA) mounted 7.5–10 m above ground on the central tower to provide nadir views (Figs. 3, 4). Images were recorded at 20–25 Hz using ResearchIR Max software, from which rate of spread, pixel ignition time, residence time, and apparent temperature were derived.

Additional surface-level observations were obtained using paired multispectral radiometers and visible-light cameras (Kremens et al., 2012, 2017) installed at 2 m height near each sonic anemometer. Radiometers sampled radiative heat flux at 1 Hz, while the cameras acquired one image per second to document flame persistence and evolution.

Fire radiative power was further characterized using "Krem Boxes" (Kremens et al., 2010, 2022), each integrating dual-band infrared radiometers, differential pressure sensors, and thermocouples at 16 locations per plot. Radiometers (Exter Research DX1001, Exergen Corporation, Watertown, MA, USA) were factory-calibrated against a blackbody reference (accuracy ±3 %) and synchronized to GPS within <50 ms. The paired differential pressure sensors (Honeywell A-HSC-D-BB-N-001ND-AA; ±250 Pa range) and type-K thermocouples provided near-probe temperature estimates and vertical convective flow indicators. All Krem Box components sampled simultaneously at 1 Hz.

3.3 Fuel, combustion, and energy release

The primary fuel used in the burns consisted of dead, dry needles from pitch pine and loblolly pine, occasionally supplemented with oak leaves or small shrubs characteristics of surface fuels in the New Jersey Pinelands. Fuel amounts added to each plot were weighted in the field using a Pesola spring scale (50 kg capacity). The target fuel loads were then uniformly distributed by hand across the 10 m x 10 m burn plots. The reported dry fuel mass was then adjusted based on the mean fuel moisture content derived from 5 - 20 subsamples collected just prior ignition. These moisture samples were placed in individual zip-lock plastic bags, kept cool in an on-site cooler, and weighted within 24 hours of collection. Samples were subsequently oven-dried at 70 °C and weighed when dry. After each fire, residual un-burned material was sampled from 3-5 0.5-m^2 subplots within the experiment plot. These residuals were oven-dried at 70 °C, manually separated into categories (pine needles, oak leaves when present, wood stems, and reproductive material) and weighed.

Fuel loading and mass loss were measured using LAUMAS ISM75 Load Cells (SN: M0179216, LAUMAS Elettronica S.r.l., Parma, Italy). Load Cells were positioned beneath the fuelbed to estimate fuel consumption and combustion rate (Figs. 3, 5). Experiments 1–26 used one cell under each of Trusses B and C, while Experiments 27–35 used two cells under Truss B.

Fuelbed structure and total fuel consumption were quantified using biometric measurements and terrestrial laser scanning (TLS) with a Faro Focus 3D X330 HDR (Faro Technologies, Lake Mary, FL, USA). TLS scans were acquired from ~2 m height at each plot corner before and after fuel placement and following each burn. Combined with biometric estimates, these data were used to calculate total energy release, while the load-cell time series captured time-resolved combustion dynamics.

https://doi.org/10.5194/essd-2026-11
Preprint. Discussion started: 16 March 2026

3.4 Gas concentration

Gas concentrations of O_2, CO_2, and CO were measured using a custom-built Transportable Analyzer for Calorimetry Outside (TACO) system (Figs. 3, 5). The system consisted of an exhaust-collection hood and duct positioned over the fuelbed, with gas samples continuously drawn from the duct. The duct radius was 0.1016 m for Burns 8–13 and 0.0508 m for Burns 14–35.

Exhaust duct pressure differential was measured using a 25 mm bi-directional probe coupled to a Sensirion SDP810-125Pa sensor. Exhaust-gas temperature was recorded with a 0.25 mm type-K thermocouple (AD8495, Analog Devices, Wilmington, MA, USA). Oxygen concentration was measured with an AO2 CiTiceL electrochemical O_2 cell, and CO/CO_2 concentrations were obtained using a non-dispersive infrared (NDIR) sensor integrated into a Crestline 7911 Automotive Gas Analyzer (Crestline Instruments, Livermore, CA, USA). All TACO data were logged at 1 Hz.

3.5 Background meteorological condition and fuel moisture

Background meteorological conditions were measured from a meteorological tower instrumented at 3 and 18 m, located approximately 50-110 m from each experimental plot. Measurements included air temperature and relative humidity (HMP45C, Vaisala Inc., Woburn, MA, USA), wind speed and direction (05013, R.M. Young Inc., Traverse City, MI) within the canopy and near the canopy top, as well as 10 h fuel moisture (CS505, Campbell Scientific, Logan, UT, USA) at 0.3 m height. These observations provided context for the in-plot measurements and enabled comparison between fire-induced and ambient atmospheric conditions. Typical pre-burn weather included air temperatures of 10–25 °C, relative humidity between 30–60 %, and winds of 2–5 m s^{-1}.

3.6 Data collection summary

All data streams were time-synchronized to GPS with sub-second precision, ensuring alignment across instruments and measurement domains. Data were continuously logged during each burn and cross-validated against redundant measurements, such as co-located temperature and pressure sensors, to verify signal integrity. Combined, these datasets provide a comprehensive, high-resolution record of fire behaviour, energy release, and environmental response suitable for advancing coupled fire–atmosphere modelling and validation efforts.

https://doi.org/10.5194/essd-2026-11
Preprint. Discussion started: 16 March 2026

Open Access Earth System Science Data Discussions

Table 1. Summary of all measurements collected during the 10 m × 10 m burns, including units, sampling rates, and the instruments used.

Data Type	**Parameter**	**Unit**	**Sampling rate (Hz)**	**Instrument**	**Model**	**Manufacture**
Fuels	Moisture	%		Gravimetric moisture		
	Structure			Terrestrial laser scanner (TLS)	Faro Focus 3D X330 HDR	Calibri
Flame characteristics	Temperature	°C	10	Thermocouple (TC)	Omega KMTXL-IOM25G-150 k	Omega Engineering
			20	IR Camera (IR)	FLIR A65SC/FOL6 100.0-650.0 C	Flir Systems
Combustion	Gas concentration (O_2, CO_2, CO)	%	1	Transportable Analyzer for Calorimetry Outside (TACO)	Crestline NDIR 7911	Crestline
	Flow velocity	m s^{-1}	1	Differential Pressure Sensor	SDP 810-125	Sensirion
	Temperature	°C	1	Type-K Thermocouple	AD8495	Analog Devices
	Mass loss	g	5	Load Cell (LC)	LAUMAS model ISM75	Levantina
Meteorology	3D wind	m s^{-1}	10	3D Sonic	RM 81000V	R. M. Young
	Virtual Temperature	°C	10	3D Sonic	RM 81000V	R. M. Young
	Air pressure	mbar	10	Pressure Sensor	BMP 180/ BMP 280	Bosch
Fire radiative power density	Net radiation	kW m^{-2}	1	Krem box (KB)		RIT
Convective vertical energy density	Convective flow	kW m^{-2}	1	Krem Box (KB)		RIT

https://doi.org/10.5194/essd-2026-11
Preprint. Discussion started: 16 March 2026

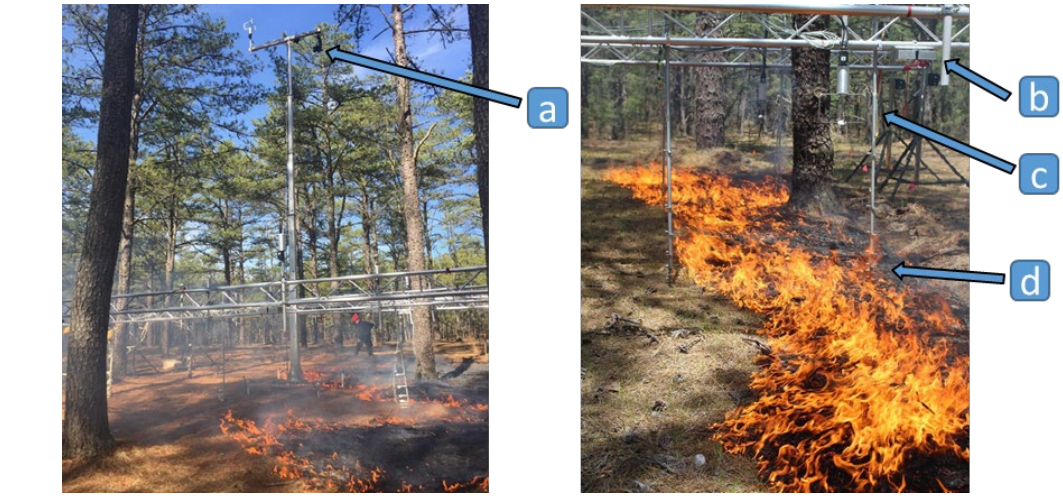

Figure 4: Trusses, central tower and instrumentation including tower-mounted (10 m) IR camera and 3D sonic anemometer (a), truss-mounted (2.5-3 m) pressure sensors (b), 3D sonic anemometers (c) and thermocouple profiles (d).

Figure 5: A closer view of instruments: Thermocouples (a), Terrestrial Lidar Scanner (b), TACO (c), Krem Box, (d), and Load Cells (e)

https://doi.org/10.5194/essd-2026-11
Preprint. Discussion started: 16 March 2026

225

4 Data processing and quality control

4.1 General data processing workflow

All datasets were subjected to standardized post-processing and quality-control procedures to ensure temporal alignment, sensor integrity, and consistency across experimental burns. Raw data from all instruments were screened for gaps, noise, 230 and signal saturation, and corrected for known sensor biases and calibration drifts using manufacturer specifications and in-field reference checks. Each dataset was synchronized to a common GPS-based time base with millisecond precision, enabling direct comparison of flow, temperature, radiation, and fuel-consumption dynamics across instruments.

Following synchronization, data were clipped to the active burn period defined by the start (AT_START) and end (AT_END) timestamps and screened for missing values, range exceedances, and anomalous diagnostic codes using 235 instrument-specific validity criteria. Outliers and physically implausible values were identified through automated filters and manual inspection, with quality flags assigned at the record level. Diagnostic flags are summarized in companion "Error.csv" files for each instrument type, reporting the percentage of missing (NaN) and suspect observations per burn. In general, a diagnostic code (DIAG) of 0 denotes valid measurements, while any other value indicates suspect or uncertain data.

All flagged data remain available in the archive but are clearly identified, allowing users to apply additional filtering as 240 appropriate for their analyses. Processed and quality-controlled data are provided in standardized formats with accompanying metadata that describe instrument configuration, calibration constants, and data-quality metrics. Figure 6 illustrates the overall data-processing workflow.

4.2 Instrument-Specific Procedures

While all instruments followed the same general workflow for synchronization, screening, and quality assurance, additional 245 instrument-specific steps were applied to account for differences in sensor response, sampling rate, and data structure. Each dataset includes a corresponding diagnostic file summarizing missing data percentages and flagging suspect records, ensuring transparency and reproducibility in downstream analyses. The following subsections describe data-processing methods and quality-control criteria applied to each instrument type

4.2.1 Sonic anemometer data

250 Three-dimensional wind velocity (u, v, w) and sonic temperature data were visually inspected for missing data segments, signal dropouts, and diagnostic code errors. Data were screened using the instrument's native diagnostic flag, where DIAG = 0 indicates valid measurements and DIAG ≠ 0 identifies suspect records due to transducer shadowing, signal loss, or saturation during intense heat flux periods.

https://doi.org/10.5194/essd-2026-11
Preprint. Discussion started: 16 March 2026

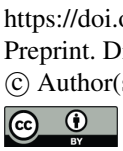

To ensure temporal consistency, data gaps were filled with missing data (NaN) symbols. Periods with more than 10% invalid samples within a 10 s window were flagged in the companion diagnostic summary file (Sonic_Error.csv, \Data\SERDP_10x10_Sonic_Raw\Sonic_Error.csv). All sonic data were synchronized to the GPS-based time base used for other instruments and clipped to the active burn period between the AT_START and AT_END timestamps.

Each record includes calibrated wind components (m s^{-1}), sonic temperature (°C), diagnostic flag, and precise GPS-synchronized timestamps. The combination of high sampling rate and rigorous QC allows the data to be used confidently in turbulence, heat flux, and fire–atmosphere coupling analyses.

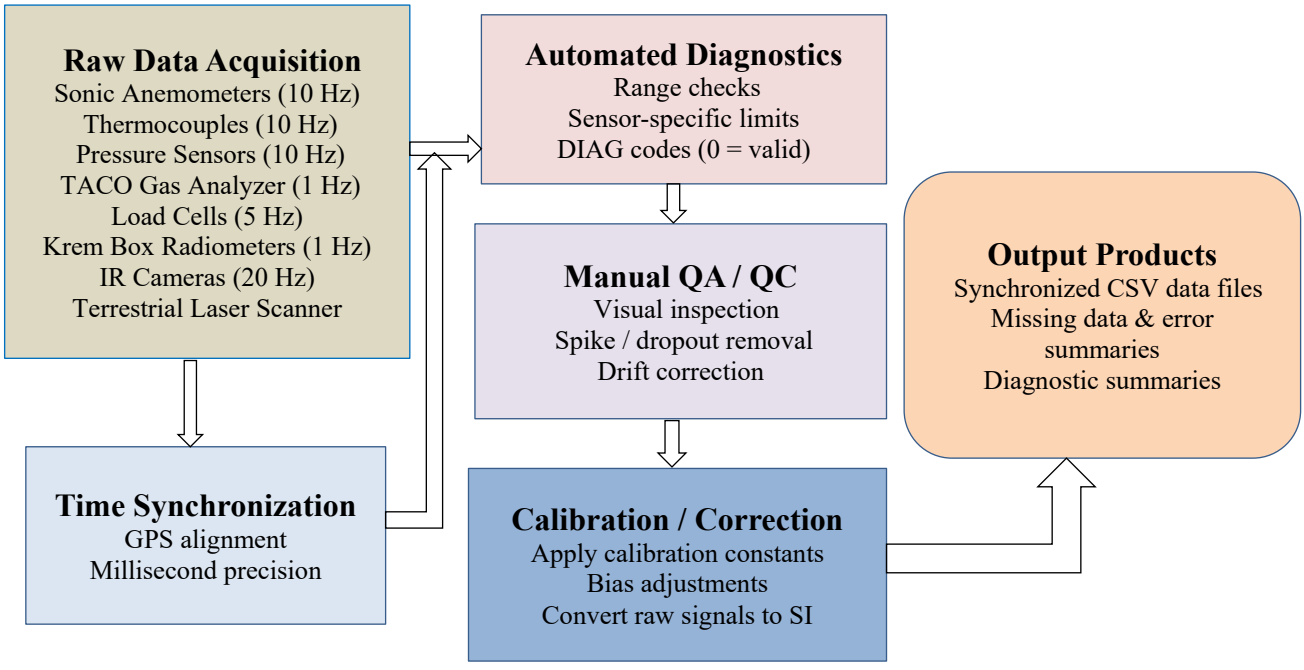

Figure 6: Data processing work flow.

4.2.2 Thermocouple and pressure data

Thermocouple data underwent manual inspection to verify signal continuity and physical plausibility. A summary file (TC_Error.csv) reports the proportion of missing and suspect data for all burns. Pressure data were evaluated against manufacturer-specified ranges, with diagnostic codes identifying suspect readings (PS_Error.csv). Users are cautioned that

https://doi.org/10.5194/essd-2026-11
Preprint. Discussion started: 16 March 2026

small inter-sensor biases may exist due to calibration drift; comparative analyses between sensors should therefore be treated with care.

4.2.3 Gas concentration measurements

Gas data from TACO were screened through a visual diagnostic process. Each burn is archived as an individual CSV file (Burn##_TACO.csv) with a companion error summary (TACO_Error.csv). The diagnostic flag DIAG = 0 identifies valid data, while DIAG = 1 marks suspect observations retained for transparency. Data processing included taking the absolute value of the measured pressure difference to correct for reversed flow direction in some burns. Occasional negative CO and CO_2 values reflect zeroing of the NDIR analyzer under ambient air conditions and minor sensor drift.

4.2.4 Fuel load and mass-loss measurements

Load cell data were visually checked for anomalies due to vibration or transient signal loss. Each burn includes a separate CSV file for each load cell (Burn##_LC_@@.csv), with corresponding error summaries in LC_Error.csv. As with other datasets, suspect values are identified through diagnostic codes but remain available for user-defined filtering.

4.2.5 Fire radiative power and convective flux

Dual-band infrared radiometer data ("Krem Box") were processed to compute radiant flux following the methods of Kremens et al. (2010), and compiled per instrument and burn (KB_Raw_Error.csv). Derived radiant-flux products are provided as condensed CSV files (Burn##_KB_RF.csv) suitable for time-series analysis of fire radiative power.

4.2.6 Infrared imagery and derived products

Infrared (IR) imagery was recorded as 20 Hz SEQ video files (Burn##_IR.seq). Every twentieth frame was extracted to create 1 Hz time-series CSVs (Burn##_IR_hhmmss00.csv). Derived products include frame lists identifying burning pixels and ignition timing (IR_FrameList_300.csv), pixel ignition time maps (IR_Ignition_300.csv), and residence-time rasters representing the duration that each pixel remained above 300 °C (IR_ResTime_300.csv). Raster products were generated from CSV outputs using LAStools (las2dem, version 200813) at 0.025 × 0.025 m spatial resolution.

4.3 Data processing and quality control summary

Across all instruments, diagnostic summary files quantify data completeness and potential quality issues, enabling rapid assessment of each burn's data integrity. While every effort was made to verify calibration and synchronization, users are advised to consult the diagnostic codes and burn metadata prior to comparative or cross-sensor analyses.

Thirty of the thirty-five burns produced complete datasets, while five burns were of insufficient intensity or had fuelbeds too wet for flames to spread fully across the burn plot. All data are archived and publicly available through the U.S.

https://doi.org/10.5194/essd-2026-11
Preprint. Discussion started: 16 March 2026

Forest Service Research Data Archive (https://www.fs.usda.gov/rds/archive/). Each dataset is accompanied by metadata, calibration records, and summary files quantifying the proportion of missing or suspect data identified through automated diagnostic screening.

Together, these standardized datasets represent one of the most comprehensive open-access records of intermediate-scale fire–atmosphere interactions available to date. Consistent file structures, synchronized timing, and transparent diagnostic coding facilitate cross-variable analyses and model validation at sub-second to plot scales. The datasets are fully documented within the U.S. Forest Service Research Data Archive and are ready for reuse in studies of combustion dynamics, energy release, and coupled fire–environment processes.

5 Applications

The field datasets collected during these fire experiments are intended to support model development, parameterization, and validation across a broad range of fire science applications. They provide comprehensive, simultaneous measurements of flow, temperature, radiation, and gas concentrations that are well suited for benchmarking physics-based, coupled fire–atmosphere models such as WFDS and FIRETEC. The data additionally enable detailed examination of combustion dynamics, including flame spread mechanisms, plume structure, and transitions between heading and backing fire behaviour. Measurements of radiative and convective heat fluxes facilitate energy-balance studies, while high-frequency observations of CO, CO_2, and O_2 concentrations allow estimation of combustion efficiency and emissions. The experiments further include fuel property measurements that link fuel structure and loading to combustion rates and flame intensity.

To demonstrate how the dataset can be applied, we present an example analysis from one of the burns in the series. Burn 21 was conducted on 20 May 2019 using hybrid pine needles (Pinus taeda × rigida) that were uniformly and loosely distributed across the plot without intentional compaction. Prior to ignition, ambient meteorological conditions included an air temperature of approximately 31 °C, relative humidity near 41%, and light southwesterly winds (≈246°) averaging about 2 m s^{-1} with gusts up to 4 m s^{-1}.

5.1 Fire spread and plume structure

Figure 7 shows a sequence of infrared (IR) images capturing the fire evolution as it propagated from west to east across the 10 m × 10 m plot under the prevailing winds. Panel (a) depicts the initial line ignition, where a fuel line treated with accelerant generates a narrow, high-temperature strip along the western boundary. As the fire progresses (panels b–f), the front expands eastward and develops a curved shape, with the central section advancing more rapidly than the northern and southern flanks. This produces a distinct bulging fire front, while the lateral edges lag behind. Over time, the overall rate of spread decreases; early frames show relatively rapid advancement (panels b–c), whereas the leading edge becomes slower and more irregular in later panels (e–f) as fuel consumption and heating alter local conditions.

https://doi.org/10.5194/essd-2026-11
Preprint. Discussion started: 16 March 2026

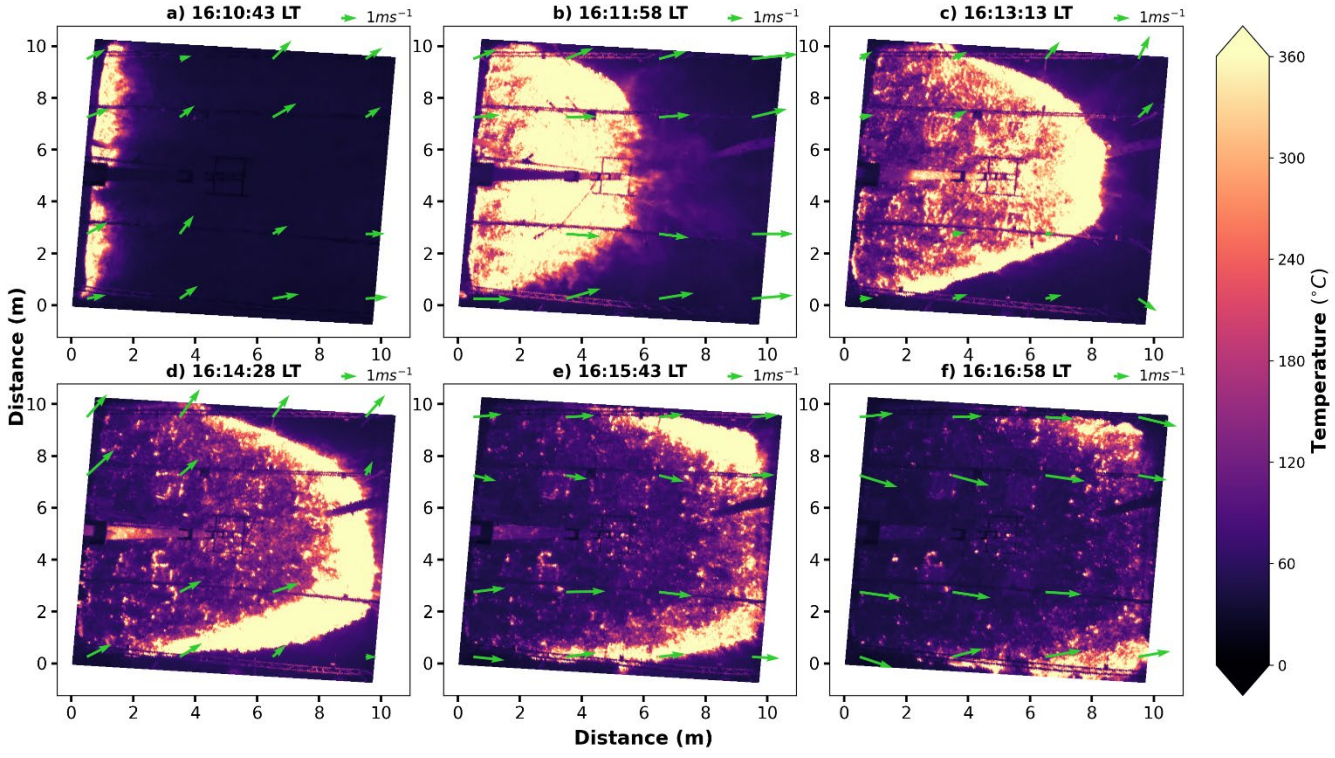

Figure 7: Temperature (shaded) observed from the IR camera on the central tower and horizontal wind velocity (green vectors) observed by the 4×4 3D sonic anemometer array (see Fig. 3) for Burn 21 on May 20, 2019.

To complement the IR imagery, Figure 7 also overlays wind vectors measured by the 4 × 4 sonic anemometer array. Although winds remain weak throughout the burn, the vectors tend to align with the direction of fire spread, consistent with the observed head-fire and flank-fire behaviour. However, there is no clear evidence of significant wind-speed enhancement induced by the fire; any fire-generated flows appear subtle relative to background variability. Overall, the combined evidence indicates that the spatial and temporal evolution of fire was governed primarily by ambient winds, the linear ignition pattern, small-scale fuel variability, and micro-flow fluctuations within the plot.

Building on the spread analysis, Figure 8 shows time series of temperatures recorded by the vertical thermocouple arrays (0–100 cm) along with sonic-anemometer temperatures at 2.5 m at 2 of the 16 sites (Fig. 3). Both sites display a distinct vertical structure in the plume. Temperatures at the upper thermocouples increase earlier and more sharply than those near the surface, indicating a forward-tilted plume as the fire front approached. This vertical structure is consistent with the increase in ambient

https://doi.org/10.5194/essd-2026-11
Preprint. Discussion started: 16 March 2026

360 wind speed with height and additional fire–atmosphere interactions that enhanced plume inclination. Peak temperatures occur immediately above the fuelbed (0–10 cm), where values reach several hundred degrees Celsius, but they diminish sharply with height. This fine vertical structure shows that the fire's influence on air temperature drops dramatically within the lowest meter, falling to much smaller magnitudes by 1 m and becoming minimal at 2.5 m. The duration of the heat pulse also broadens with height, reflecting entrainment and mixing of hot gases as the plume rises. Differences between sites B2 and C4 in peak
365 temperature and pulse width likely arise from local variability in fuel loading and flame residence time within the plot.

Together, these observations highlight the sharply stratified thermal structure of low-intensity surface fires, the rapid attenuation of heat with height, and the sensitivity of plume behaviour to fine-scale wind and fuel conditions.

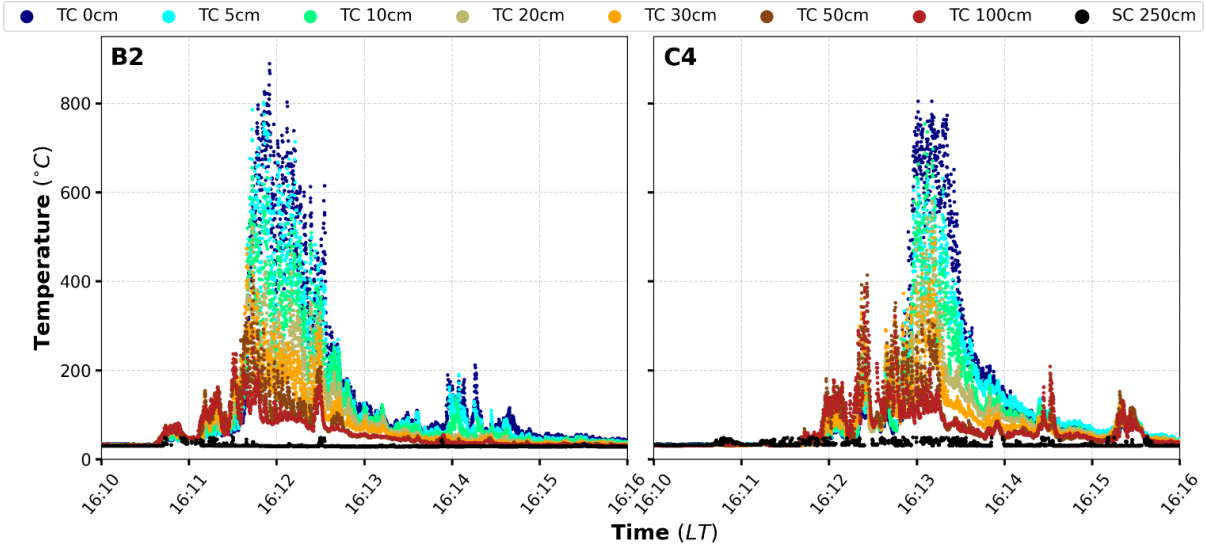

370 Figure 8. Temperature observed from the thermocouple array at two instrumented sites (B2 and C4) (See Fig. 3) during Burn 21 on May 20, 2019.

5.2 Fire-induced variability in turbulent fluxes and kinetic energy

Beyond characterizing fire spread and plume structure, the high-frequency measurements provide direct insight into how fire
375 alters heat and momentum exchange with the atmosphere. In this section, we examine fire-induced variability in turbulent momentum and heat fluxes and turbulent kinetic energy (*TKE*), highlighting the transient and highly localized atmospheric response to low-intensity surface fires.

Turbulent fluctuations φ', where φ represents u, v, w, or T, were derived from

$$\varphi' = \varphi - \overline{\varphi} \quad (1)$$

380 where the mean $\overline{\varphi}$ is calculated as average over the pre-fire period.

https://doi.org/10.5194/essd-2026-11
Preprint. Discussion started: 16 March 2026

Open Access Earth System Science Data Discussions

The measurements of horizontal wind velocity is transformed into a streamwise coordinate, in which the u-component (along wind or streamwise component) aligns with the prevailing wind direction, while the v-component (lateral or cross-stream component) is oriented perpendicular to it and directed to the left of the mean wind vector. The reference wind direction used for this rotation was calculated as average wind direction over the 10-min period immediately preceding each burn, averaged across data from all 16 sonic anemometers deployed in the array.

The *TKE* is calculated as the sum of the variance of the three perturbation velocity components:

$$TKE = \left(\overline{u'^2} + \overline{v'^2} + \overline{w'^2}\right)/2 \qquad (2)$$

where the overbars denote time averages, which in this case, was 1 min averages.

Frictional velocity u_* is a measure of turbulent shear stress or momentum flux, calculated as:

$$u_*^2 = \left(\overline{u'w'}^2 + \overline{v'w'}^2\right)^{\frac{1}{2}} \qquad (3)$$

where $\overline{u'w'}$ and $\overline{v'w'}$ represent the vertical fluxes of streamwise and cross-stream momentum flux, respectively.

Figure 9 shows box–whisker plots of the observed *TKE*, u_*, and kinematic heat flux ($H = \overline{w'T'}$) by the 16 sonic anemometers for pre-, during-, and post-burn periods. The "burn period" for this analysis was defined as the time between when the first sonic temperature exceeded 8σ (where σ is the pre-burn standard deviation) and when the last sonic temperature returned below that threshold. The 10 min before and 10 min after the fire period are referred to as pre-fire and post-fire periods.

The distributions of $\overline{w'T'}$, u_*^2, and *TKE* exhibit clear and systematic differences across the pre-burn, burn, and post-burn periods (Figure 9). During the pre-burn period, all three variables show relatively low magnitudes with narrow distributions, reflecting typical near-surface shear and turbulence levels in the absence of fire-induced disturbance.

In contrast, the burn period is characterized by substantial increases in both the medians and spreads of all three turbulence metrics. The kinematic heat flux exhibits the most dramatic change, with values increasing by more than an order of magnitude and several high-magnitude outliers exceeding 4 °C m s^{-1}. This pronounced enhancement reflects the strong buoyancy and convective activity generated by the combustion plume. Concurrently, u_*^2 also increases, with larger variability and elevated upper-range values, consistent with enhanced shear production and plume–wind interactions. *TKE* shows a similar response, with a broad distribution and peak values surpassing 3 m^2 s^{-2}, indicative of highly energetic and intermittent turbulent events within the fire environment.

Following the burn, $\overline{w'T'}$ rapidly declines toward pre-burn levels, suggesting that buoyancy production diminishes quickly once flames are extinguished. However, both u_*^2 and *TKE* remain elevated relative to their pre-burn states. The broader spread and higher median values in the post-burn period point to a persistence of enhanced shear and turbulence, potentially

https://doi.org/10.5194/essd-2026-11
Preprint. Discussion started: 16 March 2026

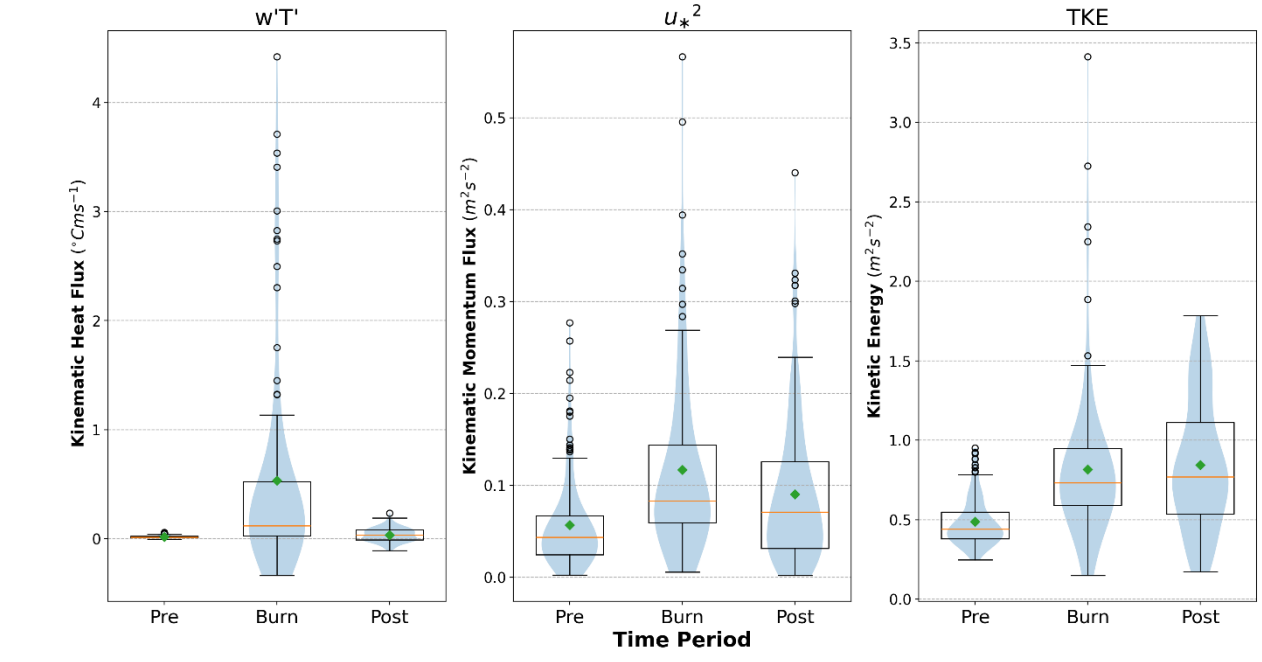

Figure 9. Distributions of kinematic heat flux ($\overline{w'T'}$), kinematic momentum flux (u_*^2), and turbulent kinetic energy (*TKE*) measured during the pre-burn, burn, and post-burn periods of Burn 21. Each panel shows combined box-and-whisker and violin plots summarizing 1-min averages of 10 Hz observations collected from the 4 × 4 sonic anemometer array. Boxes represent the interquartile range with median values indicated by orange lines; whiskers extend to 1.5× the interquartile range; individual points depict outliers; and green diamonds denote the mean.

6 Conclusions

The field experimental burns conducted on 10 m × 10 m plots provide an unprecedented, multi-sensor dataset that captures the coupled dynamics of fuels, combustion, heat transfer, and atmospheric flow under controlled yet realistic field conditions. Designed to bridge the gap between small-scale laboratory combustion studies and large operational prescribed burns, these intermediate-scale experiments combine detailed in-situ and remote measurements to quantify key processes governing fire behaviour and energy exchange across scales.

https://doi.org/10.5194/essd-2026-11
Preprint. Discussion started: 16 March 2026

A major outcome of this effort is the first synchronized, open-access collection of coupled flow–temperature–radiation observations from replicated field fires. Standardized metadata, calibration protocols, and rigorous quality-control procedures ensure data interoperability and facilitate model validation. The intermediate scale and controlled variability enable testing of fire–atmosphere coupling hypotheses and support improved parameterization of fire spread and heat flux models.

Preliminary comparisons across these intermediate-scale field experiments, small-scale controlled laboratory studies, and large-scale operational burns reveal several consistent physical relationships. Fine fuel loading, consumption, flame height, rate of spread, and energy fluxes observed during these experiments align closely with those recorded during low-intensity prescribed fires. Measurements from sonic anemometers, thermocouple arrays, and radiometers demonstrate coherent scaling of plume structure and convective fluxes, while also exposing limitations of current sensor technologies under extreme fire behaviour such as fire whirls. The experiments further highlight the need to better understand vertical and horizontal flux footprints, radiative–convective coupling, and small-scale turbulence effects on fire spread and fuel preheating.

These experiments and the resulting standardized datasets represent one of the most comprehensive open-access records of fire–atmosphere interactions to date. Their consistent structure, synchronized timing, and transparent diagnostics enable cross-variable analyses and model benchmarking from sub-second to plot scales, strengthening the empirical foundation for advancing coupled fire–atmosphere models, prescribed fire planning, and smoke emissions forecasting. Future research and analyses will extend these experiments to additional fuel types, canopy structures, and atmospheric stability regimes, integrating the observations with high-resolution numerical simulations to further improve predictive understanding of wildland fire dynamics.

7 Data Availability

All datasets and supporting documentation are publicly available through the U.S. Forest Service Research Data Archive (https://www.fs.usda.gov/rds/archive/). The data in the archive is released under the Creative Commons CC BY license (specifically Creative Commons Attribution 4.0 International License, or CC BY 4.0). The archive includes synchronized, quality-controlled measurements of fuels, wind, temperature, pressure, radiation, and combustion products collected during the field experiments. Associated files include calibration constants, processed summary data, diagnostic scripts, and detailed metadata describing sensor configurations, data formats, and quality-control procedures.

Representative datasets from this collection may be cited as, for example:

Gallagher, Michael R.; Skowronski, Nicholas S.; Hadden, Rory M.; Mueller, Eric V.; Clark, Kenneth L.; Campbell-Lochrie, Zakary J.; Walker-Ravena, Carlos; Kremens, Robert L.; Everland, Alexis I.; Patterson, Matthew M.; Cole, Jason A.; Heilman, Warren E.; Charney, Joseph J.; Bian, Xindi; Mell, William E.; Hom, John L.; Im, Seong-kyun; Kiefer, Michael T.; Zhong, Shiyuan; Simeoni, Albert J.; Rangwala, Ali; Di Cristina, Giovanni. 2022. Multi-scale analyses of wildland fire combustion

https://doi.org/10.5194/essd-2026-11
Preprint. Discussion started: 16 March 2026

processes: Small-scale field experiments – plot layout and documentation. Fort Collins, CO: Forest Service Research Data Archive. https://doi.org/10.2737/RDS-2022-0079.

Detailed information about specific data types, related references, and associated DOIs are provided in Table 2 and accompanying metadata files.

Table 2. Datasets and references

Component	Citation	DOI
Plot layout & documentation	Gallagher et al. (2022)	https://doi.org/10.2737/RDS-2022-0079
Sonic wind and temperature	Clark et al. (2022a)	https://doi.org/10.2737/RDS-2022-0081
Thermocouple temperature	Clark et al. (2022b)	https://doi.org/10.2737/RDS-2022-0083
Atmospheric Pressure	Heilman et al. (2022)	https://doi.org/10.2737/RDS-2022-0080
Fire Radiative Power	Kremens et al. (2022)	https://doi.org/10.2737/RDS-2022-0077
Fuel Loading & Consumption	Walker-Ravena et al. (2022)	https://doi.org/10.2737/RDS-2022-0078
Pre- Post-burn Biometric data	Gallagher et al. (2017)	https://doi.org/10.2737/RDS-2017-0061
TACO Gas and Flow Data	Campbell-Lochrie et al. (2022)	https//doi.org/10.2737/RDS-2022-0082
Terrestrial Laser Scanner (TLS)	Skowronski et al. (2022a)	https://doi.org/10.2737/RDS-2022-0084
Infrared images	Skowronski et al. (2022b)	https://doi.org/10.2737/RDS-2022-0076

8 Author Contributions

NS, ZC-L, KC, JC, GC, AE, MG, RH, JH, SI, RK, WM, EM, MP, AR, AS, JD, CR were responsible for instrument deployment and data acquisition. JC, MP, KC, JS were primarily responsible for data processing and quality control. JS, XB, SZ, WH, JC, NS, MK, MG and KC conducted preliminary analyses. SZ drafted the paper, with contributions from JS, MG, KC, NS, and WH. All authors contributed to experiment design.

9 Competing Interests

The authors declare that they have no conflict of interest

10 Acknowledgements

This research was supported by the Strategic Environmental Research and Development Program (SERDP Project RC-2641) of the U.S. Department of Defence. We thank the staff of the US Forest Service Northern Research Station, the Silas Little Experimental Forest and New Jersey Forest Fire Service for logistical and technical support.

https://doi.org/10.5194/essd-2026-11
Preprint. Discussion started: 16 March 2026

11 Disclaimer

Certain equipment, instruments, software, or materials, commercial or non-commercial, are identified in this paper in order to specify the experimental procedure adequately. Such identification does not imply recommendation or endorsement of any product or service, nor does it imply that the materials or equipment identified are necessarily the best available for the purpose.

12 References

Agbeshie, A. A., Abugre, S., Atta-Darkawa, T., and Awuah, R.: A review of the effects of forest fire on soil properties, J. Forest Res., 33, 1419-1441, https://doi.org/10.1007/s11676-022-01475-4, 2022.

Butler, B., Quarles, S., Standohar-Alfano, C., Morrison, M., Jimenez, D., Sopko, P., Wold, C., Bradshaw, L., Atwood, L., Landon, J., O'Brien, J., Hornsby, B., Wagenbrenner, N., and Page, W.: Exploring fire response to high wind speeds: fire rate of spread, energy release and flame residence time from fires burned in pine needle beds under winds up to 27 m s^{-1}, Int. J. Wildland Fire, 29, 81-92, https://doi.org/10.1071/WF18216, 2020.

Butler, J. D. A., Tasnia, A., Sengupta, D., Kreisberg, N., Barsanti, K. C., Goldstein, A. H., Preble, C. V., Sugrue, R. A., and Kirchstetter, T. W.: Emission factors and optical properties of black and brown carbon emitted at a mixed-conifer forest prescribed burn. EGUsphere. [preprint], https://doi.org/10.5194/egusphere-2025-2295, 2025.

Campbell-Lochrie, Z. J., Hadden, R. M., Mueller, E. V., Walker-Ravena, C., Gallagher, M. R., Clark, K. L., Hom, J. L., Kremens, R. L., Cole, J. A., Patterson, M. M., Everland, A. I., Skowronski, N. S: Multi-scale analyses of wildland fire combustion processes: Small-scale field experiments – Transportable Analyzer for Calorimetry Outside (TACO). Fort Collins, CO: Forest Service Research Data Archive. https://doi.org/10.2737/RDS-2022-0082, 2022.

Carrà, B. G., Bombino G., Lucas-Borja M. E., Plaza-Alvarez, P. A., D'Agostino D., Zema, D. A.: Prescribed fire and soil mulching with fern in Mediterranean forests: Effects on surface runoff and erosion. Ecolog. Engineer. 176, 106537, https://doi.org/10.1016/j.ecoleng.2021.106537, 2022.

Clark, K. L., Heilman, W. E., Skowronski, N. S., Gallagher, M. R., Mueller, E., Hadden, R. M., and Simeoni, A.: Fire behaviour, fuel consumption, and turbulence and energy exchange during prescribed fires in pitch pine forests. Atmos.. 11, 242, doi:10.3390/atmos11, 2020.

https://doi.org/10.5194/essd-2026-11
Preprint. Discussion started: 16 March 2026

Clark, K. L., Gallagher, M. R., Mueller, E. V., Hadden, R. M., Walker-Ravena, C., Campbell-Lochrie, Z. J., Cole, J. A., Patterson, M. M., Everland, A. I., and Skowronski, N. S.: Multi-scale analyses of wildland fire combustion processes: Small-scale field experiments - three-dimensional wind and temperature. Fort Collins, CO: Forest Service Research Data Archive, https://doi.org/10.2737/RDS-2022-0081, 2022a.

Clark, K. L., Gallagher, M. R., Mueller, E. V., Hadden, R. M., Walker-Ravena, C., Campbell-Lochrie, Z. J., Cole, J. A., Patterson, M. M., Everland, A. I., and Skowronski, N. S.: Multi-scale analyses of wildland fire combustion processes: Small-scale field experiments - temperature profile. Fort Collins, CO: Forest Service Research Data Archive. https://doi.org/10.2737/RDS-2022-0083, 2022b.

Clements, C. B., Kochanski, A. K., Seto, D., Davis, B., Camacho, C., Lareau, N. P., Contezac, J., Restaino, J., Heilman, W. E., Krueger, S. K., Butler, B., Ottmar, R. D., Vihnanek, R., Flynn, J., Filippi, J. B., Barboni, T., Hall, D. E., Mandel, J., Jenkins, M. A., O'Brien, J., Hornsby, B., and Teske, C.: The FireFlux II experiment: a model-guided field experiment to improve understanding of fire–atmosphere interactions and fire spread, Int. J. Wildland Fire, 28, 308-326. https://doi.org/10.1071/WF18089, 2019.

Cruz, M. G., Hoffman, C. M. and Fernandes, P. M.: Global synthesis of quantification of fire behaviour characteristics in forests and shrublands: Recent progress. Curr. Fores. Rep. 11, 8, https://doi.org/10.1007/s40725-024-00241-5, 2025.

Finney, M. A., Cohen, J. D., McAllister, S. S., and Jolly, W. M.: On the role of wind and moisture in the spread of wildfires in pine needle beds. Int. J. Wildland Fire, 30(6), 441–452. https://doi.org/10.1071/WF20103, 2021.

Francos, M., and Ubeda, X.: Prescribed fire management. Curr. Opin. Environ. Sci. Health, 21, 100250, https://doi.org/10.1016/j.coesh.2021.100250, 2021.

Gallagher, M. R., Clark, K. L., Thomas, J. C., Mell, W. E., Hadden, R. M., Mueller, E. V., Kremens, R. L., El Houssami, M., Filkov, A. I., Simeoni, A. J., Skowronski, N. S.: New Jersey fuel treatment effects: Pre- and post-burn biometric data. Fort Collins, CO: Forest Service Research Data Archive. https://doi.org/10.2737/RDS-2017-0061, 2017.

Gallagher, M. R., Skowronski, N. S., Hadden, R. M., Mueller, E. V., Clark, K. L., Campbell-Lochrie, Z. J., Walker-Ravena, C., Kremens, R. L., Everland, A. I., Patterson, M. M., Cole, J. A., Heilman, W. E., Charney, J. J.. Bian, X., Mell, W. E., Hom, J. L., Im, S., Kiefer, M. T., Zhong, S., Simeoni, A. J., Rangwala, Ali, Di Cristina, G.: Multi-scale analyses of wildland fire

https://doi.org/10.5194/essd-2026-11
Preprint. Discussion started: 16 March 2026

combustion processes: Small-scale field experiments – plot layout and documentation. Fort Collins, CO: Forest Service Research Data Archive. https://doi.org/10.2737/RDS-2022-0079, 2022.

Hiers, J. K., O'Brien, J. J., Varner, J. M., Butler, B. W., Dickinson, M., Furman, J., Gallagher, M., Godwin, D., Goodrick, S. L., Hood, S. M., Hudak, A., Kobziar, L. N., Linn, R. R., Loudermilk, E. L., McCaffery, S., Robertson, K., Rowell, E. M., N., Skowronski, Watts, A. C., and Yedinak, K. M.: Prescribed fire science: the case for a refined research agenda. Fire Ecol 16, 11, https://doi.org/10.1186/s42408- 020-0070-8, 2020.

Hinzman, L. D., Fukuda, M., Sandberg, D. V., Chapin III, F. S., and Dash, D.: FROSTFIRE: An experimental approach to predicting the climate feedbacks from the changing boreal fire regime. J. Geophy. Res., 108, No. D1, 8153, https://doi.org/10.1029/2001JD000415, 2003.

El Houssami, M., Thomas, J. C., Lamorlette, D., Morvan, D., Chaos, M., Hadden R., and Simeoni, A.: Experimental and numerical studies characterizing the burning dynamics of wildland fuels, Combus, and Flame, 168, 113-126, https://doi.org/10.1016/j.combustflame.2016.04.004, 2016.

Heilman, W. E., Bian, X., Clark, K. L. Skowronski, N. S., Hom, J. L., and Gallagher, M. R.: Atmospheric turbulence observations in the vicinity of surface fires in forested environments. J. Appl. Meteorol. Climatol. 56, 3133–3150, https://doi.org/10.1175/JAMC-D-17-0146.1, 2017.

Heilman, W. E., Bian, X., Clark, K. L., S., and Zhong, S.: Observations of turbulent heat and momentum fluxes during wildland fires in forested environments. J. Appl. Meteorol. Climatol. 58, 813-829, https://doi.org/10.1175/JAMC-D-18-0199.1, 2019.

Heilman, W. E., Banerjee, T. Clements, C. B., Clark, K. L., Skowronski, N. S., Zhong, S., and Bian, X.: Observations of sweep-ejection dynamics for heat and momentum fluxes during wildland fires in forested and grassland environments. J. Appl. Meteorol. Climatol. 60, 185-198. https//doi/org/10.1175/JAMC-D-20-0086.1, 2021a.

Heilman, W. E.: Atmospheric turbulence in wildland fire environments: Implication for fire behaviour and smoke dispersion. Fire Mang. Today, 79(1), 24-29, 2021b

Heilman, W. E., Skowronski, N. S., Charney. J. J., Clark, K. L., Gallagher, M. R., Hom, J. L., Zhong, S., Bian, X., Cole, J., and Patterson, M. M. 2022: Multi-scale analyses of wildland fire combustion processes: Small-scale field experiments - atmospheric pressure. Fort Collins, CO: Forest Service Research Data Archive. https://doi.org/10.2737/RDS-2022-008, 2022.

https://doi.org/10.5194/essd-2026-11
Preprint. Discussion started: 16 March 2026

Katurji, M., Noonan B., Zhang, J., Valencia, A., Shumacher, B., Kerr, J., Strand, T., Pearce, G., and Zawar-Reza, P.: Atmospheric turbulent structures and fire sweeps during shrub fires and implications for flaming zone behaviour. Int. J. Wildland Fire, 32(1) 43-55 https://doi.org/10.1071/WF22100, 2022.

Kremens, R. L., Dickinson, M., and Bova, A.: Radiant flux density, energy density and fuel consumption in mixed-oak forest surface fires. Int. J. Wildland Fire, 21, 722-730, 2012

Kremens, R. L., Skowronski, N. S., Simeoni, A. A., Clark, K. L., Mell, W. E., Hadden, R. M., Gallagher, M. R., Mueller, E.V., El Houssami, M., and Filkov, A.I.: New Jersey fuel treatment effects: Wildfire airborne sensor program-orthorectified long-wave infrared and visible data images, Fort Collins, CO: Forest Service Research Data Archive. https://doi.org/10.2737/RDS-2017-0063, 2017.

Kremens, R. L.; Gallagher, M. R., Clark, K. L., Mueller, E. V., Hadden, R. M., Heilman, W. E., Charney, J. J., Hom, J. L., Campbell-Lochrie, Z. J., Walker-Ravena, C., Everland, A. I., Cole, J. A., Patterson, M. M., and Skowronski, N. S.: Multi-scale analyses of wildland fire combustion processes: Small-scale field experiments – fire radiative power. Fort Collins, CO: Forest Service Research Data Archive. https://doi.org/10.2737/RDS-2022-0077, 2022.

Li, H., Liu N., Xie, X., Zhang, L., Yuan, X., and He, Q.: Effect of fuel bed width on upslope fire spread: An experimental study, Fire Technol. 57(3), doi: 10.1007/s10694-020-01031-8, 2020.

Li, J., Manzello, S. L., and Zhou, A.: Laboratory investigation of firebrand generation and ignition potential in wildland fuels. Fire Technol., 60(2), 789–810. https://doi.org/10.1007/s10694-023-01512-3, 2024.

Lindaas, J., Pollack, I. B., Garofalo, L. A., Pothier, M. A., Farmer, D. K., Kreidenweis, S. M., Campos, T. L., Flocke, F., Weinheimer, A. J., Montzka, D. D., Tyndall, G. S., Palm, B. B., Peng, Q., Thornton, J. A., Permar, W., Wielgasz, C., Hu, L., Ottmar, R. D., Restaino, J. C., Hudak, A. T., Ku, I.-T., Zhou, Y., Sive, B. C., Sullivan, A., Collett, J. L. Jr., and Fischer, E. V.: Emissions of reactive nitrogen from western U.S. wildfires during summer 2018, J. Geophys. Res., 126, e2020JD032657, https://doi.org/10.1029/2020JD032657, 2021.

Linn, R. R., Reisner, J., Colman, J. J., and Winterkamp, J.: Studying wildfire behaviour using FIRETEC, Int. J. Wildland Fire, 11, 233–246, https://doi.org/10.1071/WF02007, 2002.

https://doi.org/10.5194/essd-2026-11
Preprint. Discussion started: 16 March 2026

Linn, R. R., Goodrick, S. L., Brambilla, S., Brown, M. J., Middleton, R. S., O'Brien, J. J., and Hiers J. K.: QUIC-fire: A fast-running simulation tool for prescribed fire planning. Environ. Model. Softw., 125, 104616, https://doi.org/10.1016/j.envsoft.2019.104616, 2020.

Liu, Y., Kochanski, A., Liu, Y., Kochanski, Baker, K. R., Mell, W., Linn, R., Paugam, R., Mandel, J., Fournier, A., Jenkins, M, Goodrick, S., Achtemeier, G., Zhao, F., Ottmar, R., French, N., Larkin, N., Brown, T., Hudak, A., Dickinson, M., Brian, P., Clements, C., Urbanski, S., Prichard, S., Watts, A. and McNamara, D.: Fire behaviour and smoke modelling: model improvement and measurement needs for next-generation smoke research and forecasting systems, Int. J. Wildland Fire 28, 570–588, https://doi.org/10.1071/WF18204, 2019.

Mell, W., Jenkins, M. A., Gould, J., and Cheney, P.: A physics-based approach to modelling grassland fires, Int. J. Wildland Fire, 16, 1–22, https://doi.org/10.1071/WF06002, 2007.

Mueller, E. V., Skowronski, N. S., Thomas, J. C., Clark, K., Gallagher, M. R., Hadden, R., Mell, W., and Simeoni, A.: Local measurements of wildland fire dynamics in a field-scale experiment. Combus. Flame, 194, 452-463, https://doi.org/10.1016/j.combustflame.2018.05.028, 2018.

Mueller, E. V., Skowronski, N. S., and Hadden, R. M.: Smoldering combustion and emission characteristics of chaparral fuels under controlled laboratory conditions. Combus. Flame, 240, 112012, https://doi.org/10.1016/j.combustflame.2022.112012, 2022.

Ottmar, R. D., Hiers, J. K., Butler, B. W., Clements, C. B., Dickinson, M. B., Hudak, A. T., O'Brien, J. J.; Potter, B. E.; Rowell, E. M., Strand, T. M., and Zajkowski, T. J.: Measurements, datasets and preliminary results from the RxCADRE project - 2008, 2011 and 2012. Int. J. Wildland Fire 25(1):1-9., https://doi.org/10.1071/WF14161, 2016.

Prichard S., Larkin N. S., Ottmar R., French N. H., Baker K., Brown T., Clements C., Dickinson M., Hudak A., Kochanski A., Linn R., Liu Y., Potter B., Mell W., Tanzer D., Urbanski S., and Watts A.: The fire and smoke model evaluation experiment – a plan for integrated, large fire–atmosphere field campaigns. Atmos. 10, 66. doi:10.3390/ATMOS10020066, 2019.

Saha, S. and Cobian-Iñiguez, J.: Wind-driven ignition behavior of wildland fuels: Experimental insights under controlled conditions. Combus. Sci. Technol., 1–26. https://doi.org/10.1080/00102202.2025.2536215, 2025.

Seitz, J., Zhong S., Charney, J. J., Heilman, W. E., Clark, K. L., Bian, X., Skowronski, N. S., Gallagher, M. R., Patterson, M., Cole, J., Kiefer, M. T., Hadden, R. and Mueller, E.: Atmospheric turbulence observed during a fuel-bed-scale low-intensity surface fire. Atmos. Chem. Phys., 24, 1119-1142. https://doi.org/10.5194/acp-24-1119-2024, 2024.

Skowronski, N. S., Charney, J. J, Gallagher, M. R., Cole, J. A., Campbell-Lochrie, Z. J., Walker-Ravena, C., Mueller, E. V., Everland, A. I., Patterson, M. M.: Multi-scale analyses of wildland fire combustion processes: Small-scale field experiments – terrestrial laser scans. Fort Collins, CO: Forest Service Research Data Archive. https://doi.org/10.2737/RDS-2022-0084, 2022a.

Skowronski, N. S., Charney, J. J, Clark, K. L., Gallagher, M. R., Hadden, R. M., Heilman, W. E., Hom, J. L., Kremens, R. L., Cole, J. A., Campbell-Lochrie, Z. J., Walker-Ravena, C., Mueller, E. V., Everland, A. I. : Multi-scale analyses of wildland fire combustion processes: Small-scale field experiments – infrared data. Fort Collins, CO: Forest Service Research Data Archive. https://doi.org/10.2737/RDS-2022-0076, 2022b.

Valko, A. and Deak, B.: Increasing the potential of prescribed burning for the biodiversity conservation of European grasslands, Cur. Opinion in Environ, Sci. & Health, 22, 100268, https://doi.org/10.1016/j.coesh.2021.100268, 2021.

Walker-Ravena, C., Hadden, R. M., Mueller, E. V., Campbell-Lochrie, Z. J., Gallagher, M. R., Cole, J. A., Patterson, M. M., Skowronski, N. S.: Multi-scale analyses of wildland fire combustion processes: Small-scale field experiments – fuel loading and consumption. Fort Collins, CO: Forest Service Research Data Archive. https://doi.org/10.2737/RDS-2022-0078. 2022.